Transactions on Engineering Sciences vol 6, © 1994 WIT Press, www.witpress.com, ISSN 1743-3533

Viscoplastic-microdamage constitutive modeling of dynamic fracture

J. Eftis,[a] J.A. Nemes[b]

[a] *Department of Civil, Mechanical and Environmental Engineering, George Washington University, Washington D.C. 20052, USA*

[b] *Department of Mechanical Engineering, McGill University, Montreal, PQ, Canada H3A 2K6*

ABSTRACT

Spall type fracture of a circular plate caused by mechanical impact and high strain rate fracture of a tensile bar caused by dynamic load application are described using a viscoplastic-damage type of constitutive model. Identification of the microvoid volume fraction of polycrystalline materials as a microdamage scalar field variable, and inclusion into an elastic-viscoplastic constitutive theory enables description of rate-dependent compressible inelastic deformation that includes material degradation culminating in fracture. Calculations simulating the spall fracture and fragmentation of a circular plate induced by high velocity impact, and the necking localization and fracture at high strain rate of a dynamically loaded smooth tensile bar, are shown.

INTRODUCTION

Spallation is a particular form of dynamic fracture that results from the development of extreme tensile mean stress carried by propagation of waves of rarefaction. A schematic of spall fracture is shown by Fig. 1. The impact of the thinner flyer plate with the stationary target plate creates a compressive stress wave that travels across the target thickness, and is reflected back at the rear surface as a tensile stress wave moving in the opposite direction. A similar process, but in reversed direction, occurs within the flyer plate. The superimposing within the target of the two tensile wave fronts coming from opposite directions, if of sufficient intensity, causes instantaneous separation of the target material along a plane perpendicular to the direction of the wave fronts. Much information describing the physical aspects of spall and dynamic fracture can be found in the review articles by Curran, Seaman & Shockey [1], and Meyers & Aimone [2].

By means of a viscoplastic-microdamage type of constitutive model the authors have been able to simulate spall fracture of a rectangular plate subject to

normal and to oblique types of impact [3-6], the spallation and fragmentation of a circular plate [7], and the necking localization and fracture of a dynamically loaded uniform tensile bar [8]. Space limitation permits discussion of the main results of two of the four studies.

SUMMARY OF THE CONSTITUTIVE EQUATIONS

A summary of the elastic-viscoplastic-damage rate type of constitutive equations are listed below. Discussion of the material parameters and their values appropriate for the OFHC copper material employed in the calculations can be found in references [3,4]. Linear decomposition of the elastic and viscoplastic rates of deformation is assumed, $\mathbf{D}=\mathbf{D}^e+\mathbf{D}^p$. The elastic deformation is assumed to be of small order so that

$$\boldsymbol{D}^e=\frac{1}{2\bar{\mu}}\left[\check{\boldsymbol{T}}-\frac{\bar{\nu}}{1+\bar{\nu}}(tr\check{\boldsymbol{T}})\mathbf{1}\right], \tag{1}$$

$\check{\boldsymbol{T}}$ is an objective stress rate of the Cauchy stress tensor $\mathbf{T}$, the elastic constants

$$\bar{\mu}(\xi) = \mu(1-\xi)\left(1-\frac{6K+12\mu}{9K+8\mu}\xi\right),\ \bar{K}(\xi)=\frac{4\mu K(1-\xi)}{4\mu+3K\xi},\ \bar{\nu}=\frac{1}{2}\frac{3\bar{K}-2\bar{\mu}}{3\bar{K}+\bar{\mu}} \tag{2}$$

where $\xi=(V-V_s)/V$ is the microvoid volume fraction, V_s is the solid volume portion of the total volume V, μ and K are the elastic shear and bulk moduli for the solid material without voids. The rate of viscoplastic deformation

$$\boldsymbol{D}^p=\frac{\gamma_0}{\phi}\left[\frac{J_2'+n\xi J_1^2}{\left[q+(\kappa_0-q)e^{-\beta e^p}\right]^2\left[1-(\xi/\xi_F)^{1/2}\right]^2}-1\right]^{m_1}\frac{1}{\kappa_0}\left(2n\xi J_1\mathbf{1}+\boldsymbol{T}'\right). \tag{3}$$

$\mathbf{T}'$ is the deviator of the stress tensor, stress invariants $J_1=trT$, and $J_2'=1/2tr(\boldsymbol{T}'\cdot\boldsymbol{T}')$, $\phi\left[\left(I_2/I_2^s\right)-1\right]^m$ where $I_2=\|II_D^{1/2}\|$, $II_D=\frac{1}{2}\left[(trD)^2-tr(\boldsymbol{D}\cdot\boldsymbol{D})\right]$, I_2^s is the quasi-static value of the rate of deformation invariant. κ_0 is the rate-independent uniaxial stress, q and β are the isotropic strain hardening parameters, $e^p=\int_o^t 2/\sqrt{3}\|II_D^{1/2}\|dt$ is the equivalent plastic strain invariant, γ_0 is the macro-viscosity of the material, and n,m,m_1 are material parameters. The rate of increase of the microvoid volume fraction is given by [5]

$$\dot{\xi}=\frac{h(\xi)}{1-\xi}\left[\exp\left(\frac{m_2|\sigma-\sigma_N|}{\kappa\theta}\right)-1\right]+\frac{1}{\eta}g(\xi)F(\xi,\xi_0)(\sigma-\sigma_G),\ \begin{matrix}\sigma>\sigma_N\\ \sigma>\sigma_G\end{matrix}, \tag{4}$$

where $\sigma=(1/3)trT$, ξ_0 is the initial microvoid volume fraction,

$$F(\xi,\xi_0)=\frac{\sqrt{3}}{2}\xi\left(\frac{1-\xi}{1-\xi_0}\right)^{2/3}\left[\xi-\left(\frac{\xi}{\xi_0}\right)^{2/3}\right]^{-1},\quad \sigma_G=\frac{1}{\sqrt{3}}(1-\xi)\ln\left(\frac{1}{\xi}\right)\left[2q+(\kappa_0-q)F_1(\xi,\xi_0)\right] \tag{5}$$

$$F_1(\xi,\xi_0)=\exp\left[\frac{2}{3}\beta\frac{(\xi-\xi_0)}{\xi(1-\xi_0)}\left(\frac{1-\xi}{1-\xi_0}\right)^{-2/3}\left(\frac{\xi_0}{\xi}\right)^{-2/3}\right]+\exp\left[\frac{2}{3}\beta\frac{(\xi_0-\xi)}{(1-\xi_0)}\left(\frac{1-\xi}{1-\xi_0}\right)^{-2/3}\right]. \tag{6}$$

The mean stress σ_N and σ_G are the threshold values for void nucleation and growth, θ is the temperature, κ is the Boltzmann constant, $h(\xi)$ and $g(\xi)$ are material functions, η and m_2 are microviscosity and void nucleation material parameters. A local criteria for fracture is defined by attainment of a critical value $\xi=\xi_F$ for the microvoid volume fraction.

SPALL FRACTURE OF A CIRCULAR PLATE

For the circular plate configuration shown by Fig. 2, impact produces compressive plane wave fronts propagating across each plate, as well as a non-planar wave starting from the circular edge of the smaller flyer, traveling radially in towards the center. For thickness dimensions that are small compared to diameters, the central region of the target will briefly experience high tensile mean stress from the superposition of the reflected plane waves prior to arrival of the radial edge wave, which if sufficiently large cause spall fracture at the interior. The physical features of the failure, i.e., the location of the spall plane, the diameter of the separated circular region, and whether or not the target will develop a 'scab', or experience fragmentation, depends upon the relative diameters and thicknesses of the colliding plates, as well as the flyer velocity. The detailed equations of motion, constitutive equations and boundary conditions are shown in reference [7]. The plate dimensions used in the calculations are for the flyer, radius 20mm., thickness 3mm., and for the target, radius 40mm., thickness 6mm. With the z-axis taken along the thickness of the plate, Fig. 3 shows the locations of the contours for the normal stress T_{zz} at 6000 MPa and for the shear stress T_{rz} at 150 MPa, at 0.5, 1.0 and 1.5μs following impact at 350 m/s. The inward moment of the vertical edge of the normal stress contour indicates the interaction of the planar compressive-reflected tensile wave with the nonplanar shear wave from the edge of the flyer moving radially in toward the center and across the target thickness. This would seem to indicate why the diameter of the spall surface is initially smaller than the diameter of the flyer.

Onset of damage, determined by an increase of the microvoid volume fraction, occurs at an impact velocity of approximately 50 m/s. The effect of further increasing the impact velocity is shown in Figures 4(a)-4(c) at 5μs after impact. (For illustrative purposes the deformation in the vertical direction has been magnified by a factor of three). The corresponding microvoid volume distribution across the target is shown by Fig. 5. At 100 m/s impact damage has taken place, however the void volume fraction is well below the critical value for copper at $\xi_F=0.32$. The material softening that accompanies the void growth is illustrated by the elongation of the mesh elements across the mid-plane. This becomes more evident at 200 m/s impact velocity where the void volume fraction approaches 0.32 over the mid-plane region,

implying fracture across the mid-plane. At 350 m/s impact the rear spalled section of the target has sufficient momentum to cause further widening of the opening in the plate.

Figure 6 illustrates the post spall deformation of the target at 5μs, 15μs and 50μs following impact at 350 m/s. In this test simulation the flyer plate thickness has been reduced to one-quarter the thickness of the target, causing the spall plane to move further back from the impact face from mid-plane to three fourths the distance to the rear surface. (In figures 6 and 7 the vertical deformations have not been magnified as in Figures 4(a)-4(c). Also, the element deletion capability available in the computer code has been utilized). Calculations beyond 50μs post impact show no significant changes, indicating a 'scab' type spall failure. When the flyer thickness is increased to one-half the target thickness the spall plane occurs at the mid-plane of the target after an impact at 350 m/s, as shown by Fig. 7. At 5μs post impact spall has developed along the mid-plane, with the rear portion of the fractured segment moving out away from the remainder of the plate with momentum sufficient to maintain the outward motion. This leads to fracture at the edges of the spall at 15μs. By 50μs the spalled segment has detached fragmenting the plate. Subsequent calculation shows no further fracture of the segment.

DYNAMIC FRACTURE OF A TENSILE BAR

The geometry of the smooth cylindrical tensile bar is shown in Fig. 8. Dynamic loading conditions were simulated by applying velocities to the upper end of the bar along the outer diameter using a ramp history with the applied velocity $U = U_o\ (t/t_o)$ having a rise time of 50μs as shown in Fig. 8. Simulations were conducted using values of U_o equal to 10, 25, 50 and 100 m/s, giving rise to nominal strain rates over the gage length of 500, 1,2500, 2,500 and 5,000 s^{-1}. A discussion of the values used for the material parameters for the copper material, and an exposition of the detailed constitutive equation, equations of motion and boundary conditions are given in reference [8].

The conditions pertaining to the stress and deformation of a tensile bar at high strain rate differ considerably from that at low rates, where the inertial effects of particle acceleration and wave propagation are negligible. During the early stages of a dynamic tensile test the stress and deformation are not uniformly distributed. The dynamic heterogeneity leads to stress and strain localization and necking at different locations of the smooth bar in the absence of geometrical or material irregularities often times used to induce necking at particular locations. This can be seen by the numerical results tabulated in Fig. 9, where it is shown that the calculated positions of strain localization along the gage section are directly influenced by the loading rate. At a nominal strain rate of 5,000 s^{-1} localization occurs 7.04 mm above the specimen centerline, whereas at 2,500 s^{-1} the necking appears at 5.38 mm below the centerline. For strain rate at 1,250 s^{-1} two necked areas appear 3.31 mm above and below the centerline. Only at the lowest strain rate considered, at 5 x 10^2 s^{-1}, did localization take place at the centerline of the bar. Correspondingly for strain rates at this level and below, the calculated load and displacement curves (not included here) show no signs of inertial effects, i.e. wave propagation. Figures 10 and 11 exhibit contours for the axial and radial stress components T_{zz} and T_{rr}, and the equivalent plastic strain ϵ^p, at 150μs, 200μs and

250μs after load initiation. These contours are at the neck location 7.04 mm above the gage centerline corresponding to the imposed strain rate at $5x10^3s^{-1}$. Over a time interval of 100μs, they show the stress and equivalent plastic strain at first developing at the center of the bar and growing towards the circumferential edge before localizing to a narrow band of high stress and large plastic deformation. These figures give some indication of the temporal features associated with dynamic spatial localization, and the dramatic changes that take place from 200μs to 250μs after start of the loading process where the highest levels for the longitudinal and radial stress develop at the center of the bar over a very narrow band. Simultaneously there is a rapid development of the neck profile with intensification and spatial concentration of the stress. Fig. 12 shows the contours of the void volume fraction at 235μs and 245μs after load initiation. The void growth begins where the tensile mean stress is greatest, at the center of the bar, extending radially outward towards the surface, attaining highest values along the plane of minimum cross-section. This suggests that the material separation will initially resemble a penny shaped crack growing radially from the center to the circumferential edge. The fractured surfaces of the bar are delineated by Fig. 13, which shows a nonplanar feature near the outer edge that approximately resembles the 'shear lip' common to the ductile fracture of round bars.

REFERENCES

1. Curran, D.R. Seaman, L., and Shockey, D.A., 'Dynamic Failure of Solids.' Physic Reports, vol. 147 (5/6), pp 253-388, 1987.
2. Meyers, M.A., and Aimone, C., 'Dynamic Fracture (Spalling) of Metals', Prog. in Mater. Sci., Vol. 28 (1), pp 1-96, 1983.
3. Nemes, J.A., Eftis, J., and Randles, P.W., 'Viscoplastic Constitutive Modeling of High Strain-Rate Deformation, Material Damage, and Spall Fracture', ASME J. Appl. Mech., Vol. 57, pp. 282-291, 1990.
4. Eftis, J., Nemes, J.A., and Randles, P.W., 'Viscoplastic Analysis of Plate-Impact Spallation', Int. J. Plasticity, Vol. 7, pp 15-39, 1991.
5. Eftis, J., and Nemes, J.A., 'Evolution Equation for the Void Volume Growth Rate in a Viscoplastic-Damage Constitutive Model', Int. J. Plasticity, Vol. 7, pp 275-293, 1991.
6. Nemes, J.A., and Eftis, J., 'Pressure-Shear Waves and Spall Fracture Described by a Viscoplastic-Damage Constitutive Model', Int. J. Plasticity, Vol. 8, pp. 185-207, 1992.
7. Eftis, J., and Nemes, J.A., 'Modeling of Impact-Induced Spall Fracture and Post Spall Behavior', Int. J. Fracture, Vol. 53, pp 301-321, 1992.
8. Nemes, J.A., and Eftis, J., 'Constitutive Modeling of the Dynamic Fracture of Smooth Tensile Bars', Int. J. Plasticity, Vol. 9, pp. 243-270, 1993.

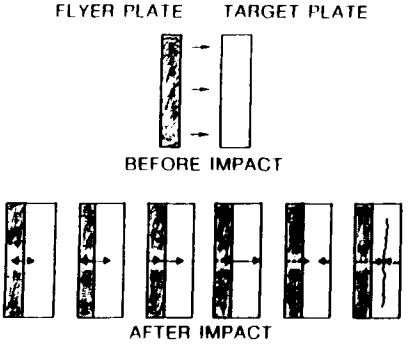

Figure 1. Spall fracture induced by plate impact.

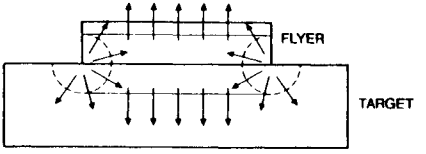

Figure 2. Circular plate impact.

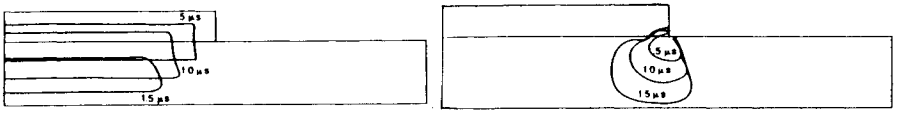

Figure 3. Time variation of the stress contours for T_{zz}=6000MPa and T_{rz}=150MPa, respectively, for plate impact at 350m/s.

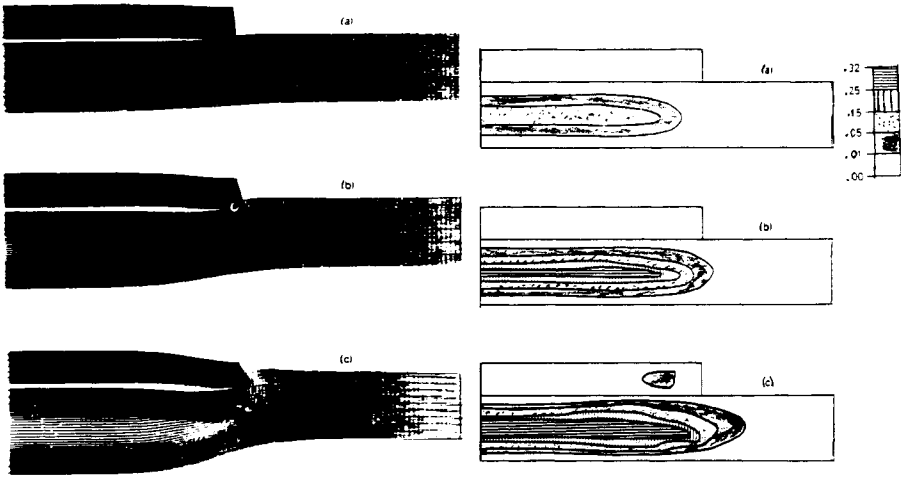

Figure 4. Target plate configuration 5μs after impact for flyer plate velocities at (a) 100m/s, (b) 200m/s, (c) 350m/s.

Figure 5. Contours for microvoid volume fraction 5μs after impact for flyer plate velocities at (a) 100 m/s, (b) 200 m/s, (c) 350 m/s.

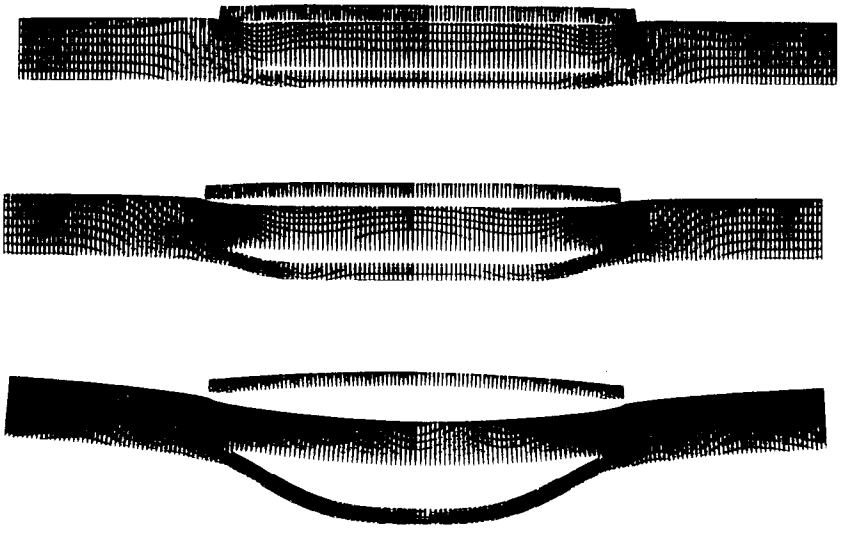

Figure 6. Spall fracture configurations at 5μs, 15μs and 50μs, respectively, after impact at 350 m/s velocity.

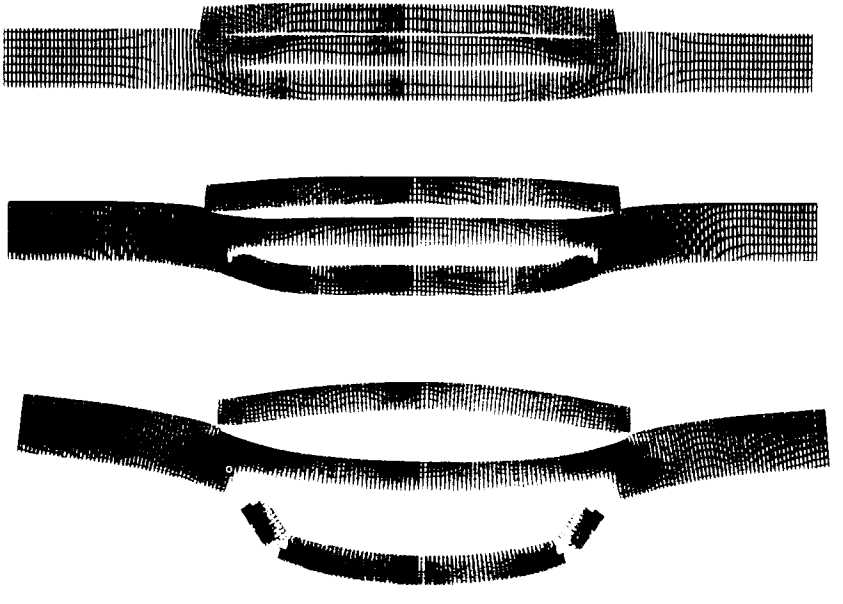

Figure 7. Spall fracture and fragmentation at 5μs, 15μs, 50μs, respectively, after impact at 350 m/s velocity with a thicker flyer plate.

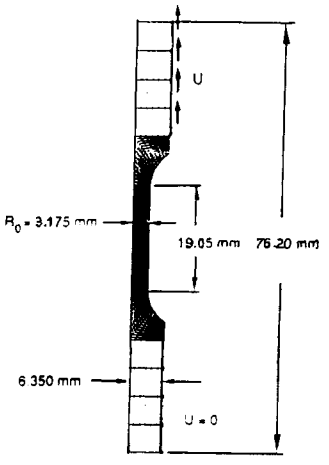

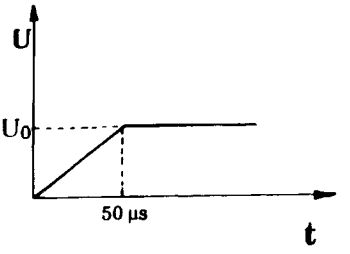

U_0	Nom Strain Rate
100	5000 s^{-1}
50	2500 s^{-1}
25	1250 s^{-1}
10	500 s^{-1}

Figure 8. Tensile bar geometry.
Imposed end velocity loading rate and gage section nominal strain rates.

Neck Location as a Function of Rate

APPLIED VELOCITY	NOMINAL RATE	NECK LOCATION
100 m/s	5000 s^{-1}	7.04 mm⇑
50 m/s	2500 s^{-1}	5.38 mm⇓
25 m/s	1250 s^{-1}	3.31 mm⇑ 3.31 mm⇓
10 m/s	500 s^{-1}	CL

Figure 9. Gage neck location referred to gage center line as related to the imposed loading rates.

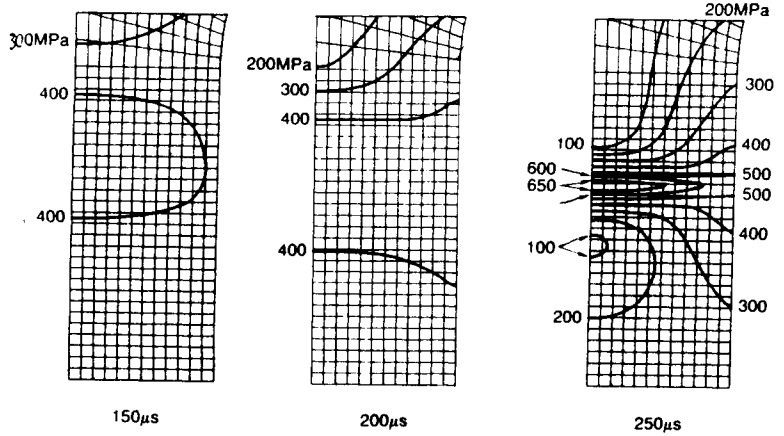

Figure 10. Contours for the axial stress component T_{zz} at 150μs, 200μs and 250μs after load initiation, showing the localization at the 7.04 mm neck location.

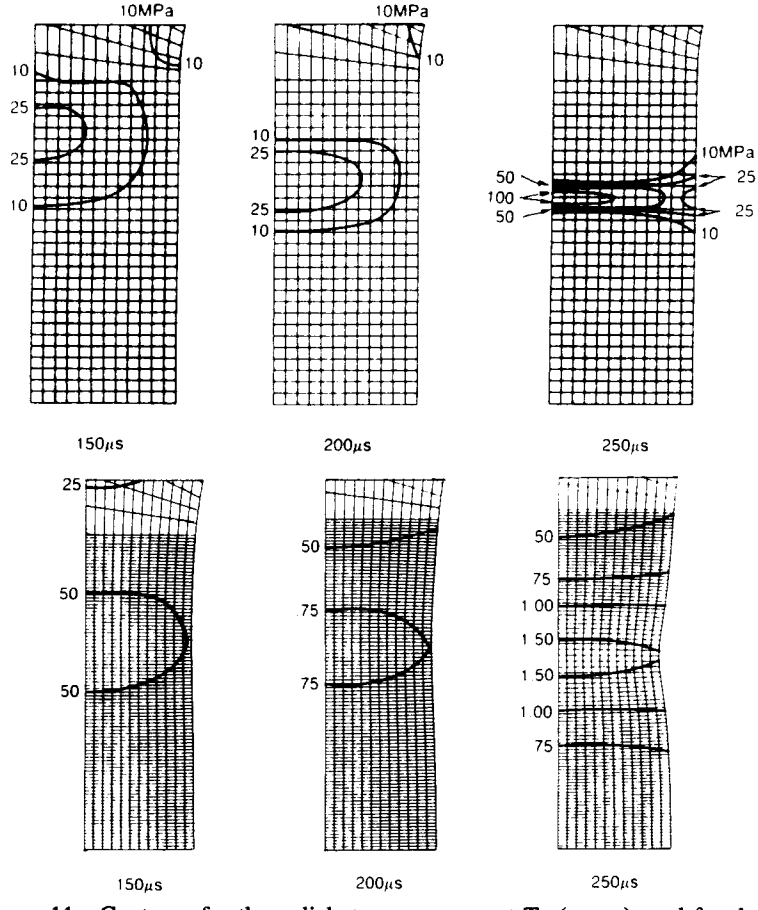

Figure 11. Contours for the radial stress component T_{rr} (upper), and for the equivalent plastic strain e^p (lower), at 150μs, 200μs and 250μs after load initiation, showing the localization at the 7.04 mm neck location.

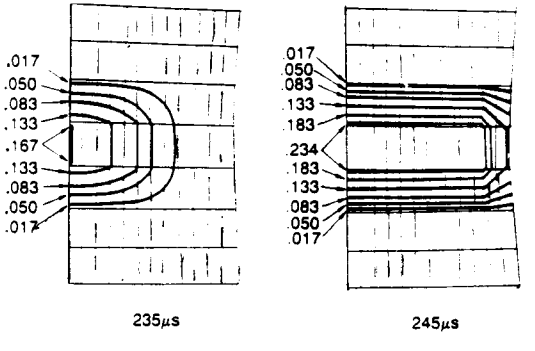

Figure 12. Contours for the microvoid volume fraction at the 7.04 mm neck location at 235μs and 245μs after load initiation.

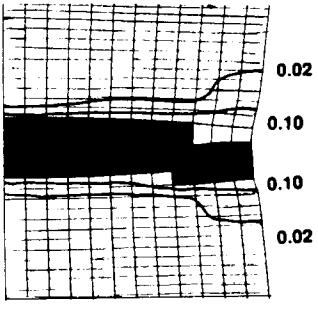

Figure 13. Deleted mesh elements delineating fracture surfaces & microvoid volume fraction contours.